

Journal of Mechanics of Materials and Structures

**ANALYTICAL APPROACH TO THE PROBLEM OF AN AUXETIC LAYER
UNDER A SPATIALLY PERIODIC LOAD**

Henryk Kamiński and Paweł Fritzkowski

Volume 13, No. 4

July 2018



ANALYTICAL APPROACH TO THE PROBLEM OF AN AUXETIC LAYER UNDER A SPATIALLY PERIODIC LOAD

HENRYK KAMIŃSKI AND PAWEŁ FRITZKOWSKI

The problem of an infinite elastic layer under a periodic load is considered. A mathematical model is formulated for the plane strain state. An analytical procedure based on the Fourier integral transformation is discussed. The displacement components are obtained as infinite sums directly via the inverse Fourier transform. Semianalytical results are presented in a nondimensional form for the case of conventional elastic materials (positive Poisson's ratio) and auxetic materials (negative Poisson's ratio). The deformation of the loaded boundary and other characteristic surfaces of the layer is analyzed, and the displacement and stress fields are demonstrated. The effect of Poisson's ratio on the system behavior is studied. The results are compared with the purely numerical solutions obtained using the finite element method.

1. Introduction

Nowadays, in times of advanced numerical methods and modern simulation software, the classical mathematical modeling and analytical treatment of formulated problems seem to belong to the past. Engineers and researchers almost automatically reach for powerful computer tools, even if an analytical approach could be applied easily. Beyond any doubt, most of the contemporary problems in computational mechanics are of a complex nature due to their geometry as well as the load and constraint conditions. However, often an analytical solution to a simplified model may become a strong base for further studies of more sophisticated and realistic systems.

In the field of linear elasticity, many fundamental problems have been formulated on strong assumptions. For instance, an unbounded (fully or partially) character of a domain (e.g., elastic space/plane, half-space/plane, elastic layer or strip) and/or a specific case of stress-strain state (plane stress/strain) have been considered. Such an approach has allowed for analytical treatment of the problems by means of the complex potentials method, integral transforms, Fourier series, and stress functions, etc. [Teodorescu 2013; Sadd 2004; Saada 1974; Nowacki 1970; Timoshenko and Goodier 1951].

In fact, exact solutions have significant advantages over the numerical ones. First of all, they facilitate a qualitative analysis of a given problem and enable one to draw more general conclusions. Secondly, analytical solutions play a role of a reference point for brand new or improved computational methods and algorithms. Moreover, the analytical approach may be useful for simulation studies of more complex or unconventional systems. A good example are auxetics, i.e., materials with negative Poisson's ratio. Analytical solutions to purely theoretical problems can cast new light on unusual deformation behavior of auxetic systems with numerous potential applications [Evans and Alderson 2000; Prawoto 2012; Alderson and Alderson 2007; Fritzkowski and Kamiński 2016; Sanami et al. 2014; Carneiro et al. 2013].

This work has been supported by 02/21/DSPB/3477 and 02/21/DSPB/3493 grants.

Keywords: linear elasticity, elastic layer, deformation, auxetic materials, Fourier transform, approximate methods.

It should be noted that, although auxetics have been known since the 1980s, their properties (mechanical, thermal, and others) and mechanisms of the anomalous deformation still draw attention of many researchers. However, a significant majority of the studies are based on the purely numerical approach (e.g., see [Walczak et al. 2014; Strek et al. 2010; Jopek and Strek 2015; Salit and Weller 2009]).

This paper is devoted to stress and deformation analysis of an elastic solid layer subjected to a spatially periodic load. Since a state of plane strain is assumed, the problem is reduced to a two-dimensional one. The displacement field equations are solved by a semianalytical approach, i.e., the Fourier integral transform is applied in combination with numerical evaluation of the displacement and stress components. The main aim of this work is to investigate the effect of Poisson's ratio on the behavior of the elastic system.

The paper is divided into five sections. In Section 2, a mathematical formulation of the elasticity problem is presented. The semianalytical solution procedure is presented in Section 3. Section 4, in turn, contains simulation results and discussion. Finally, some conclusions and closing remarks are provided in Section 5.

2. Formulation of the problem

Let us consider the elastic layer illustrated in Figure 1. The term “layer” should be understood as a part of an elastic space (infinite domain) bounded by two parallel planes at a finite distance h [Teodorescu 2013]. The upper boundary face (xz) is subjected to a distributed normal load $p(x)$ which is periodic along the x -axis:

$$p(x) = p(x + 2a). \quad (2-1)$$

The solid material that occupies the domain is assumed to be linearly elastic, homogeneous, and isotropic. It is characterized by shear modulus G and Poisson's ratio ν . In the case of auxetics, $\nu < 0$.

Taking into account the domain and loading geometry (independent of the z coordinate), the spatial problem can be reduced to a two-dimensional formulation. The specified case falls into the category of plane strain problems, and consequently we focus on a semiinfinite planar region

$$\Omega = \begin{cases} -\infty \leq x < \infty, \\ -h \leq y \leq 0. \end{cases} \quad (2-2)$$

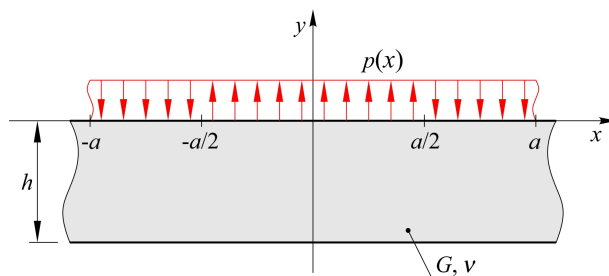


Figure 1. Infinite elastic layer under a periodic load.

Let $\mathbf{u}(x, y) = [u_x, u_y]^T$ be the displacement vector. The strain-displacement relations involving only the allowable strains are given by

$$\varepsilon_x = \frac{\partial u_x}{\partial x}, \quad \varepsilon_y = \frac{\partial u_y}{\partial y}, \quad \varepsilon_{xy} = \frac{1}{2} \left(\frac{\partial u_x}{\partial y} + \frac{\partial u_y}{\partial x} \right). \quad (2-3)$$

From Hooke's law, the corresponding stress components become

$$\sigma_x = \lambda(\varepsilon_x + \varepsilon_y) + 2\mu\varepsilon_x, \quad \sigma_y = \lambda(\varepsilon_x + \varepsilon_y) + 2\mu\varepsilon_y, \quad \sigma_{xy} = 2\mu\varepsilon_{xy}, \quad (2-4)$$

where λ and μ are Lamé constants, given as

$$\lambda = \frac{2G\nu}{1-2\nu}, \quad \mu = G. \quad (2-5)$$

Finally, in the case of zero body forces, the Navier–Lamé equations reduce to [Nowacki 1970; Sadd 2004]

$$\mu \nabla^2 u_x + (\lambda + \mu) \frac{\partial}{\partial x} \left(\frac{\partial u_x}{\partial x} + \frac{\partial u_y}{\partial y} \right) = 0, \quad (2-6a)$$

$$\mu \nabla^2 u_y + (\lambda + \mu) \frac{\partial}{\partial y} \left(\frac{\partial u_x}{\partial x} + \frac{\partial u_y}{\partial y} \right) = 0. \quad (2-6b)$$

Moreover, for the given problem, the unknown vector-valued function $\mathbf{u}(x, y)$ must satisfy the following traction boundary conditions:

$$\sigma_y(x, 0) = p(x), \quad (2-7a)$$

$$\sigma_{xy}(x, 0) = 0, \quad (2-7b)$$

$$\sigma_y(x, -h) = 0, \quad (2-7c)$$

$$\sigma_{xy}(x, -h) = 0. \quad (2-7d)$$

Thus, the resulting mathematical model consists of the system of coupled partial differential equations (2-6) together with the set of boundary conditions (2-7).

3. Analytical solution procedure

3.1. Transformation of the problem. Let $f(x)$ be a real function of a real variable x , which satisfies Dirichlet's conditions and is absolutely integrable. For further purposes, the following definition of the Fourier integral transform of f is used [Bronsztajn et al. 2004; Sneddon 1951; Teodorescu 2013]:

$$\mathcal{F}[f(x)] = \int_{-\infty}^{\infty} f(x) e^{-isx} dx, \quad (3-1)$$

where the variable s is real.

Now, let \tilde{u}_x and \tilde{u}_y denote the Fourier transforms of the displacements with respect to the x -coordinate, that is,

$$\tilde{u}_x(s, y) = \mathcal{F}_x[u_x(x, y)], \quad \tilde{u}_y(s, y) = \mathcal{F}_x[u_y(x, y)]. \quad (3-2)$$

Taking the transform of the governing equations (2-6), one can obtain

$$(\kappa - 1) \frac{\partial^2 \tilde{u}_x}{\partial y^2} + i2s \frac{\partial \tilde{u}_y}{\partial y} - s^2(\kappa + 1) \tilde{u}_x = 0, \quad (3-3a)$$

$$(\kappa + 1) \frac{\partial^2 \tilde{u}_y}{\partial y^2} + i2s \frac{\partial \tilde{u}_x}{\partial y} - s^2(\kappa - 1) \tilde{u}_y = 0, \quad (3-3b)$$

where κ denotes the Kolosov constant:

$$\kappa = 3 - 4\nu. \quad (3-4)$$

It should be noticed that these equations have simpler form than the original ones.

Next, consider the boundary conditions (2-7). Let $p_b(x)$ be a basis function of the distributed load, i.e., the load over one period ($-a \leq x \leq a$), so that periodic summation can be used:

$$p(x) = \sum_{k=-\infty}^{\infty} p_b(x - 2ka). \quad (3-5)$$

In the given case

$$p_b(x) = p_0 \left[-\eta(x + a) + 2\eta\left(x + \frac{1}{2}a\right) - 2\eta\left(x - \frac{1}{2}a\right) + \eta(x - a) \right], \quad (3-6)$$

where p_0 is the load intensity and η denotes the Heaviside step function. The Fourier transform of (3-6) is given by

$$\tilde{p}_b(s) = \frac{ip_0}{s} [e^{isa} - e^{-isa} + 2e^{isa/2} - 2e^{-isa/2}]. \quad (3-7)$$

Taking into account formula (3-5) as well as the linearity and shifting (translation) properties of the Fourier transform, for the whole periodic load applied to the infinite boundary one can write [Bronsztajn et al. 2004; Zemanian 1965]

$$\tilde{p}(s) = \tilde{p}_b(s) \sum_{k=-\infty}^{\infty} e^{-i2kas}. \quad (3-8)$$

Now, boundary conditions (2-7) can be converted to

$$\tilde{\sigma}_y(s, 0) = \tilde{p}(s), \quad (3-9a)$$

$$\tilde{\sigma}_{xy}(s, 0) = 0, \quad (3-9b)$$

$$\tilde{\sigma}_y(s, -h) = 0, \quad (3-9c)$$

$$\tilde{\sigma}_{xy}(s, -h) = 0, \quad (3-9d)$$

where

$$\tilde{\sigma}_x(s, y) = \mathcal{F}_x[\sigma_x(x, y)],$$

$$\tilde{\sigma}_y(s, y) = \mathcal{F}_x[\sigma_y(x, y)],$$

$$\tilde{\sigma}_{xy}(s, y) = \mathcal{F}_x[\sigma_{xy}(x, y)].$$

To sum up, after the transformation the boundary value problem is composed of the equilibrium equations (3-3) and associated boundary conditions (3-9).

3.2. Solution of the transformed problem. Due to its relatively simple form, the transformed problem can be solved in a quite conventional way. For the second-order partial differential equations (3-3), the trial solution is

$$\tilde{u}_x(s, y) = C_1 e^{ry}, \quad \tilde{u}_y(s, y) = C_2 e^{ry}, \quad (3-10)$$

where C_1 and C_2 are real constants, while r is generally a complex parameter to be determined. Inserting (3-10) into the homogeneous system (3-3) leads to a characteristic equation for r . There are two double roots:

$$r_{1,2} = s, \quad r_{3,4} = -s,$$

thus, the general solution is given by

$$\tilde{u}_x(s, y) = A_{11}e^{sy} + A_{12}ye^{sy} + B_{11}e^{-sy} + B_{12}ye^{-sy}, \quad (3-11a)$$

$$\tilde{u}_y(s, y) = A_{21}e^{sy} + A_{22}ye^{sy} + B_{21}e^{-sy} + B_{22}ye^{-sy}, \quad (3-11b)$$

where A_{ij} , B_{ij} (for $i, j = 1, 2$) are complex constants. Substituting \tilde{u}_x and \tilde{u}_y into (3-3), one obtains

$$\alpha_{11}e^{sy} + \alpha_{12}ye^{sy} + \beta_{11}e^{-sy} + \beta_{12}ye^{-sy} = 0, \quad (3-12a)$$

$$\alpha_{21}e^{sy} + \alpha_{22}ye^{sy} + \beta_{21}e^{-sy} + \beta_{22}ye^{-sy} = 0, \quad (3-12b)$$

where α_{ij} , β_{ij} (for $i, j = 1, 2$) denote certain functions of s and y , involving the constants A_{ij} , B_{ij} . Equating to zero the coefficients α_{ij} and β_{ij} , one can find that system (3-12) is fulfilled (for every s and y) if

$$A_{12} = iA_{22}, \quad B_{22} = iB_{12} \quad (3-13)$$

and

$$B_{12} = -\frac{s}{\kappa}(iB_{21} + B_{11}), \quad A_{22} = -\frac{s}{\kappa}(iA_{11} + A_{21}). \quad (3-14)$$

Now, the transformed displacements with four independent constants are

$$\tilde{u}_x(s, y) = \left[A_{11} + (A_{11} - iA_{21})\frac{sy}{\kappa} \right] e^{sy} + \left[B_{11} - (B_{11} + iB_{21})\frac{sy}{\kappa} \right] e^{-sy}, \quad (3-15a)$$

$$\tilde{u}_y(s, y) = \left[A_{21} - (A_{21} + iA_{11})\frac{sy}{\kappa} \right] e^{sy} + \left[B_{21} + (B_{21} - iB_{11})\frac{sy}{\kappa} \right] e^{-sy}. \quad (3-15b)$$

The constants can be determined from the prescribed boundary conditions. Obviously, it is necessary to use relations (2-3) and (2-4) to express $\tilde{\sigma}_y$, $\tilde{\sigma}_{xy}$ in terms of \tilde{u}_x , \tilde{u}_y . The traction conditions (3-9a) and (3-9b) require

$$\begin{aligned} A_{21} &= -\frac{\tilde{p}(s)e^{2hs}[4h^2s^2 - (\kappa + 1)(e^{2hs} + 2hs - 1)]}{4Gs[e^{4hs} - 2e^{2hs}(1 + 2h^2s^2) + 1]}, \\ B_{21} &= \frac{\tilde{p}(s)e^{2hs}[4h^2s^2 - (\kappa + 1)(e^{-2hs} - 2hs - 1)]}{4Gs[e^{4hs} - 2e^{2hs}(1 + 2h^2s^2) + 1]}. \end{aligned} \quad (3-16)$$

Then, conditions (3-9c) and (3-9d) lead to

$$\begin{aligned} A_{11} &= -\frac{i[2\kappa B_{21}e^{2hs} - A_{21}(4h^2s^2 + 4\kappa hs + \kappa^2 + 1)]}{4h^2s^2 - \kappa^2 + 1}, \\ B_{11} &= \frac{i[2\kappa A_{21}e^{-2hs} - B_{21}(4h^2s^2 - 4\kappa hs + \kappa^2 + 1)]}{4h^2s^2 - \kappa^2 + 1}. \end{aligned} \quad (3-17)$$

On the basis of (3-15) together with relationships (3-16) and (3-17), one can find expressions for the Fourier transforms of the displacement components:

$$\tilde{u}_x(s, y) = \frac{i\tilde{p}(s)}{4G} \frac{\phi_x(s, y)}{\psi(s, y)}, \quad \tilde{u}_y(s, y) = \frac{\tilde{p}(s)}{4G} \frac{\phi_y(s, y)}{\psi(s, y)}, \quad (3-18)$$

where

$$\begin{aligned} \phi_x(s, y) &= A_1 \sinh(sy) + A_2 \sinh(s(y + 2h)) + B_1 \cosh(sy) + B_2 \cosh(s(y + 2h)), \\ \phi_y(s, y) &= B'_1 \sinh(sy) + B'_2 \sinh(s(y + 2h)) + A'_1 \cosh(sy) + A'_2 \cosh(s(y + 2h)), \\ \psi(s, y) &= s[2h^2s^2 - \cosh(2hs) + 1], \end{aligned} \quad (3-19)$$

and

$$\begin{aligned} A_1 &= -2s(y - \kappa h + h), & A_2 &= 2sy, & A'_1 &= -2s(y + \kappa h + h), \\ B_1 &= 4hs^2(y + h) - \kappa + 1, & B_2 &= \kappa - 1, & B'_1 &= 4hs^2(y + h) + \kappa + 1, & B'_2 &= -\kappa - 1. \end{aligned}$$

These results can be subjected to the inverse Fourier transformation in order to obtain the unknown displacements u_x and u_y as well as the stresses and strains.

3.3. Inverse transformation. In view of the definition (3-1), the corresponding inverse Fourier transform is represented by [Bronsztejn et al. 2004; Sneddon 1951; Teodorescu 2013]

$$f(x) = \mathcal{F}^{-1}[\tilde{f}(s)] = \frac{1}{2\pi} \int_{-\infty}^{\infty} \tilde{f}(s) e^{isx} ds. \quad (3-20)$$

In computational practice, direct evaluation of the above integral is usually complicated (if possible), and therefore is rarely conducted. However, this approach can be used in the case under investigation.

It is clear from (3-18) that the complexity of the inversion procedure is mainly affected by the form of the image function $\tilde{p}(s)$. To simplify the calculations, Poisson's summation formula is applied [Zemanian 1965]:

$$\sum_{k=-\infty}^{\infty} e^{iks} = 2\pi \sum_{k=-\infty}^{\infty} \delta(s - 2\pi k), \quad (3-21)$$

where δ denotes the Dirac delta function. Hence, the expression (3-8) can be written alternatively as

$$\tilde{p}(s) = \frac{\pi}{a} \tilde{p}_b(s) \sum_{k=-\infty}^{\infty} \delta\left(s - \frac{\pi k}{a}\right). \quad (3-22)$$

According to the general definition (3-20), the inverse Fourier transforms of (3-18) are

$$u_x(x, y) = \frac{1}{2\pi} \int_{-\infty}^{\infty} \frac{i\tilde{p}(s)}{4G} \frac{\phi_x(s, y)}{\psi(s, y)} e^{isx} ds, \quad u_y(x, y) = \frac{1}{2\pi} \int_{-\infty}^{\infty} \frac{\tilde{p}(s)}{4G} \frac{\phi_y(s, y)}{\psi(s, y)} e^{isx} ds. \quad (3-23)$$

Substituting (3-22) into (3-23), converting (3-7) to trigonometric form, and taking into account the sifting property of the Dirac delta leads to the following result:

$$u_x(x, y) = \frac{2ip_0}{Ga} \sum_{k=-\infty}^{\infty} \sin^3\left(\frac{1}{4}as_k\right) \cos\left(\frac{1}{4}as_k\right) \frac{\phi_x(s_k, y)}{s_k \psi(s_k, y)} e^{is_k x}, \quad (3-24a)$$

$$u_y(x, y) = \frac{2p_0}{Ga} \sum_{k=-\infty}^{\infty} \sin^3\left(\frac{1}{4}as_k\right) \cos\left(\frac{1}{4}as_k\right) \frac{\phi_y(s_k, y)}{s_k \psi(s_k, y)} e^{is_k x}, \quad (3-24b)$$

where $s_k = \pi k/a$. Finally, after some manipulations and observations, one can find

$$u_x(x, y) = \frac{p_0}{Ga} \sum_{k=1}^{\infty} (-1)^k \sin(s'_k x) \frac{\phi_x(s'_k, y)}{s'_k \psi(s'_k, y)}, \quad (3-25a)$$

$$u_y(x, y) = -\frac{p_0}{Ga} \sum_{k=1}^{\infty} (-1)^k \cos(s'_k x) \frac{\phi_y(s'_k, y)}{s'_k \psi(s'_k, y)}, \quad (3-25b)$$

where $s'_k = s_{2k-1} = \pi(2k-1)/a$. The displacements can be used to determine the strain and stress components by means of the relations (2-3) and (2-4).

For example, the full form of the k -th term for the horizontal displacement is

$$u_{xk} = \frac{(-1)^k p_0 \sin(s'_k x)}{Gas_k'^2 [2h^2 s_k'^2 - \cosh(2hs'_k) + 1]} \left[-2s'_k(y - \kappa h + h) \sinh(s'_k y) + 2s'_k y \sinh(s'_k(y + 2h)) \right. \\ \left. + (4hs_k'^2(y + h) - \kappa + 1) \cosh(s'_k y) + (\kappa - 1) \cosh(s'_k(y + 2h)) \right]. \quad (3-26)$$

Similarly, the k -th term for the normal stress σ_x , for instance, can be written as

$$\sigma_{xk} = \frac{4(-1)^k p_0 \cos(s'_k x)}{as_k'^2 [2h^2 s_k'^2 - \cosh(2hs'_k) + 1]} \left[-s'_k(y - 2h) \sinh(s'_k y) + s'_k y \sinh(s'_k(y + 2h)) \right. \\ \left. + (2hs_k'^2(y + h) - 1) \cosh(s'_k y) + \cosh(s'_k(y + 2h)) \right]. \quad (3-27)$$

As can be seen from the sample analytical results, the expressions for the displacement components naturally involve Poisson's ratio ν (via the constant κ), while the stress field is independent of the parameter.

4. Simulation results

4.1. Semianalytical results. The results reported below have been obtained for the special case when $a/h = 1$. For natural reasons, in numerical computations the infinite sums in formulae (3-25) are truncated to a finite number of terms:

$$u_x(x, y) \approx \sum_{k=1}^n u_{xk}, \quad u_y(x, y) \approx \sum_{k=1}^n u_{yk}. \quad (4-1)$$

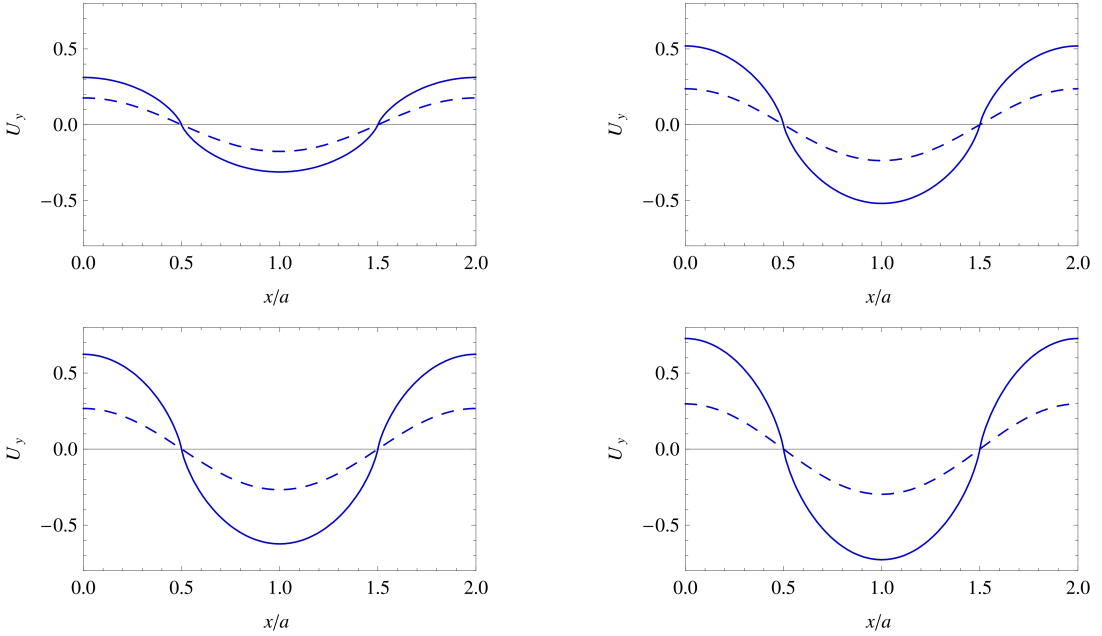


Figure 2. Vertical displacement of the loaded surface (solid) and the midsurface (dashed) for various values of Poisson's ratio. Top left: $\nu = 0.25$. Top right: $\nu = -0.25$. Bottom left: $\nu = -0.5$. Bottom right: $\nu = -0.75$. Results obtained for $n = 50$.

Moreover, the results have a nondimensional form. More precisely, the dimensionless displacements are introduced as

$$U_x(x, y) = \frac{G}{p_0 a} u_x(x, y), \quad U_y(x, y) = \frac{G}{p_0 a} u_y(x, y). \quad (4-2)$$

Analogously, the following nondimensional stresses are defined as

$$S_x(x, y) = \frac{1}{p_0} \sigma_x(x, y), \quad S_y(x, y) = \frac{1}{p_0} \sigma_y(x, y), \quad S_{xy}(x, y) = \frac{1}{p_0} \sigma_{xy}(x, y). \quad (4-3)$$

Let us start with a displacement analysis of the layer. In [Figure 2](#) the vertical displacements U_y of the loaded surface ($y = 0$) and the midsurface ($y = -h/2$) for $0 \leq x \leq 2a$ are presented for various values of Poisson's ratio. For ease of comparison, all the graphs have equal axis scales. The deformation behavior is intuitively reasonable and qualitatively identical in each case. The maximum absolute values, $\max |U_y|$, occur at $x = ka$ for $k = 0, 1, 2, \dots$, i.e., in the middle of each subinterval of the upward or downward load. As can be seen, the values grow with decreasingly lower ν . The surfaces have zero displacement at $x = (2k - 1)a$ for $k = 1, 2, \dots$, where the load changes its direction.

Similar plots for the horizontal displacement are shown in [Figure 3](#). Now, the maximum absolute values, $\max |U_x|$, arise at $x = (2k - 1)a$ for $k = 1, 2, \dots$, while zero values can be observed at $x = ka$ for $k = 0, 1, 2, \dots$. However, the displacements of the midsurface are much smaller, and a change of sign occurs as Poisson's ratio is decreased.

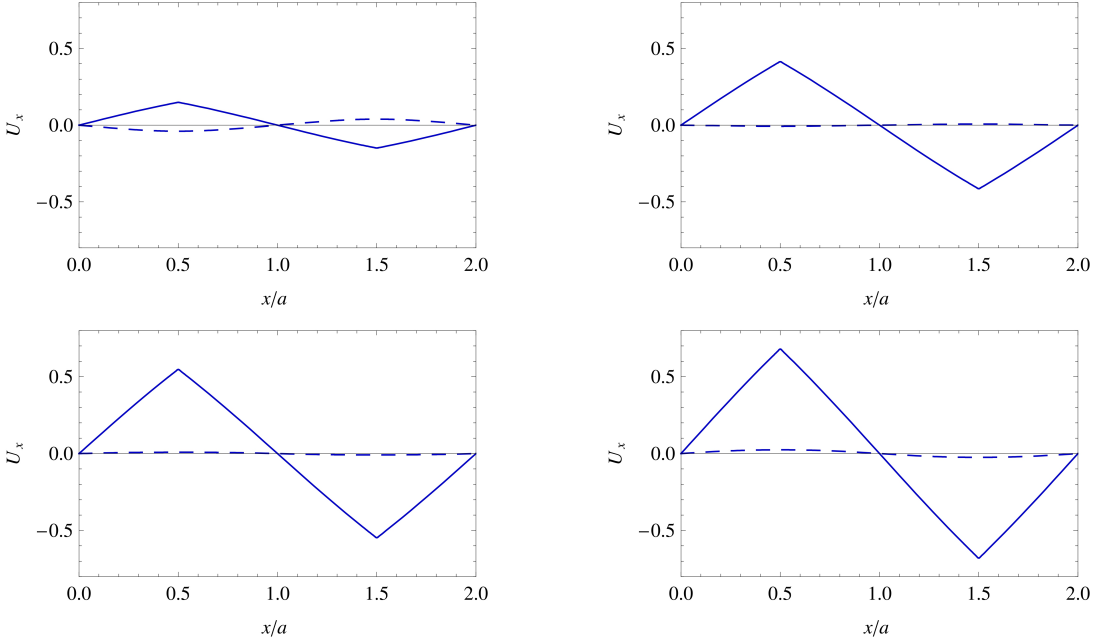


Figure 3. Horizontal displacement of the loaded surface (solid) and the midsurface (dashed) for various values of Poisson's ratio. Top left: $\nu = 0.25$. Top right: $\nu = -0.25$. Bottom left: $\nu = -0.5$. Bottom right: $\nu = -0.75$. Results obtained for $n = 50$.

To give a more systematic insight into changes of the displacements when ν is varied, the following quantities are used:

$$U_y^{\max} = U_y|_{x=0}, \quad U_x^{\max} = U_x|_{x=a/2}$$

The functions $U_y^{\max}(\nu)$ and $U_x^{\max}(\nu)$ related to the top-, mid- and bottom-surface of the layer are presented in Figure 4. As can be seen, the maximum vertical displacement for all the surfaces is always positive and increases linearly with decreasing Poisson's ratio. The character of U_x^{\max} is also linear. However, the midsurface has near zero displacement, while in case of the bottom-surface the displacement is negative and it decreases with decreasing ν .

The discussed results have been obtained for $n = 50$. This number of terms of the analytical solution ensures a good approximation of the layer displacements. The maximal values U_y^{\max} in the function of n for selected values of Poisson's ratio are plotted in Figure 5. As can be seen, the results converge rapidly, and for $n > 50$ there are no significant deviations in U_y^{\max} . It should be noted that over the whole analyzed range ($10 \leq n \leq 200$) the displacement values differ by less than 0.15%.

Let us turn to an overall look at the displacement field. Figure 6 shows the distribution of the horizontal and vertical displacements (scaled by a factor of 10^2) within an elementary cell of the layer: $\langle 0, 2a \rangle \times \langle -h, 0 \rangle$, for three values of Poisson's ratio: $\nu = 0.25$, $\nu = -0.25$ and $\nu = -0.5$. When it comes to U_x , there are two types of zero isolines: vertical (at $x = a$) and approximately horizontal. Position of the latter one is affected by ν . In the case of a conventional material ($\nu > 0$), one can observe an evident disproportion between the area above and below the contour of zero value. In the distribution of U_y , there

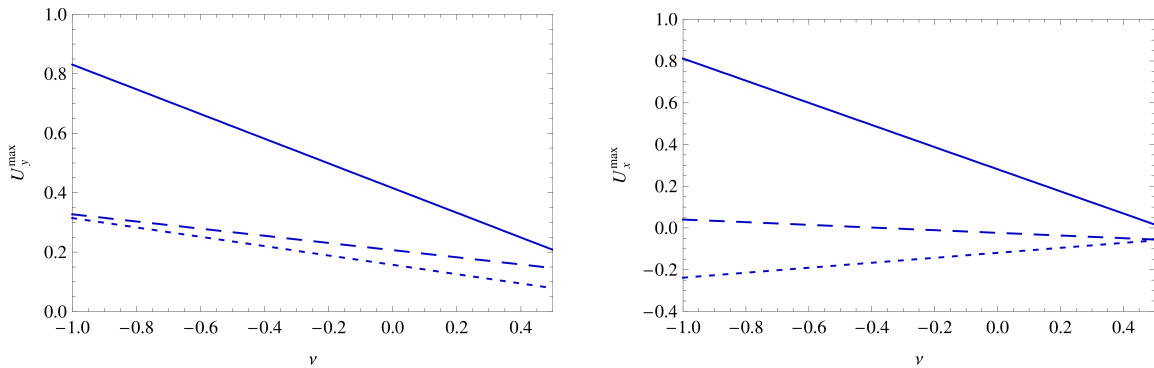


Figure 4. Maximal vertical (left) and horizontal (right) displacements versus Poisson's ratio for the surfaces at $y = 0$ (solid), $y = -h/2$ (dashed), and $y = -h$ (dotted). Results obtained for $n = 50$.

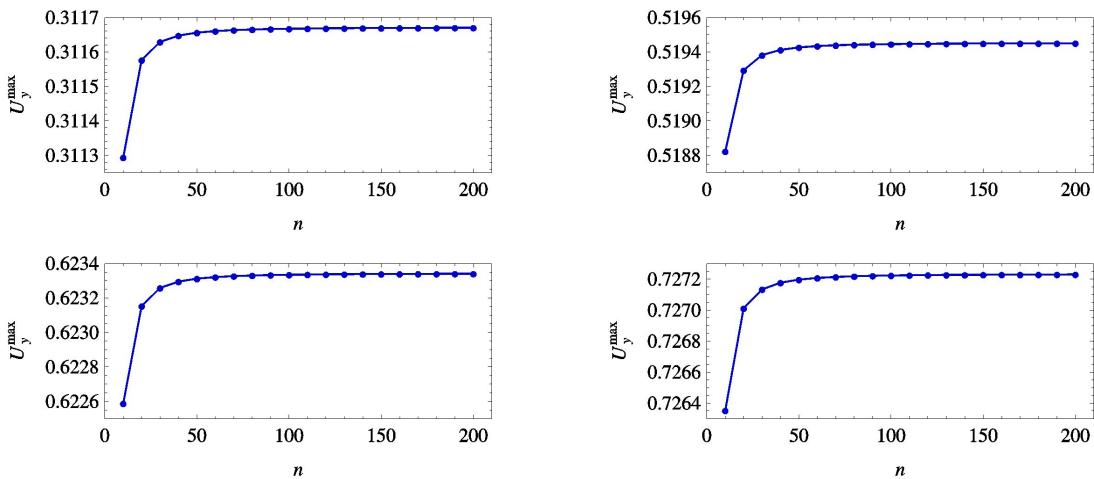


Figure 5. Approximated value of the maximal vertical displacement versus the number of summed terms of the analytical solution for various values of Poisson's ratio. Top left: $\nu = 0.25$. Top right: $\nu = -0.25$. Bottom left: $\nu = -0.5$. Bottom right: $\nu = -0.75$.

are only vertical zero isolines (at $x = a/2$ and $x = 3a/2$). Some differences arise in their neighborhood: the nearby contours become increasingly barrel-shaped as Poisson's ratio is decreased.

The longitudinal displacement (U_x) of the cell through its thickness is plotted in Figure 7. More precisely, the curves that represent the layer cross-sectional deplanation at $x = a/4$ (or $x = 3a/4$) and $x = a/2$ are presented for selected values of Poisson's ratio. As can be seen from Figure 3 and Figure 6, $U_x(x, y) = 0$ for every y at $x = 0$, $x = a$, $x = 2a$. The displacement profiles at $x = 5a/4$ (or $x = 7a/4$) and $x = 3a/2$, in turn, are mirror images of the respective curves for $x = a/4$ (or $x = 3a/4$) and $x = a/2$ about the central transverse axis $x = a$.

Although the displacements increase with decreasing ν (see Figure 3), all the curves intersect at one point. Its location can be found based on (3-26). Since the second and the next terms of the series (4-1) decay strongly, they are negligible compared with the first term. Now, for two arbitrary values of the

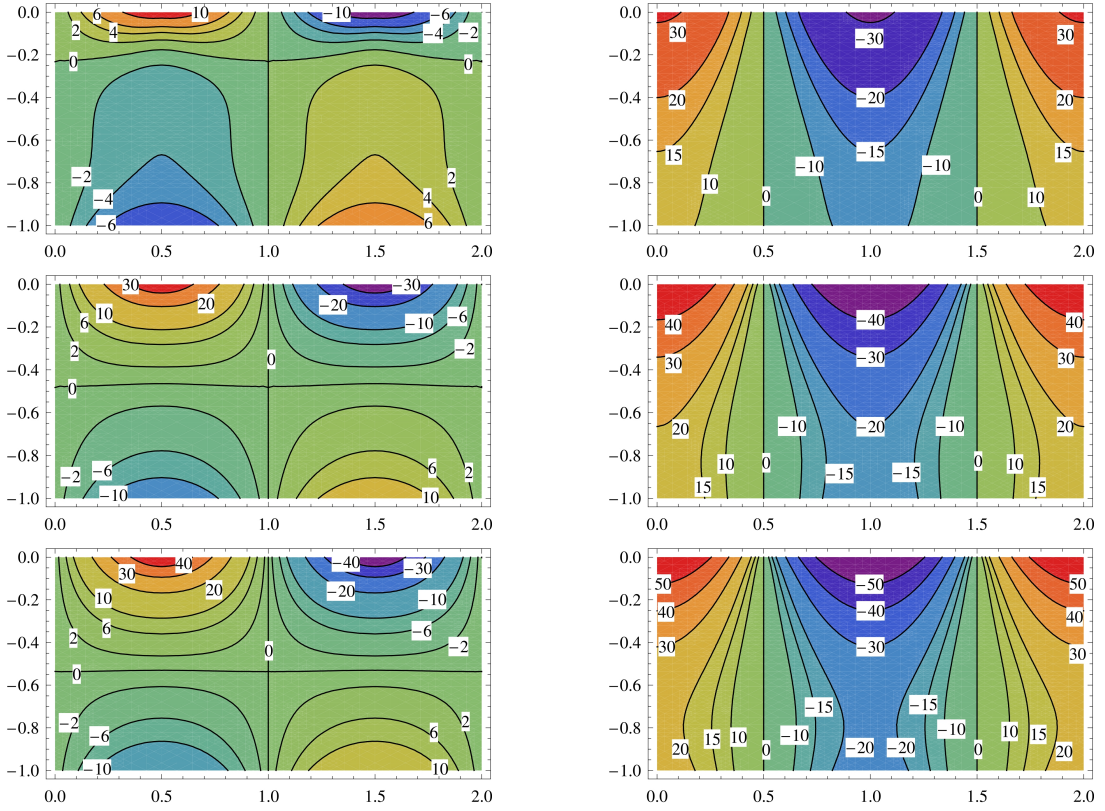


Figure 6. Displacement distribution in a rectangular cell — horizontal displacement $U_x \times 10^2$ (left column) and vertical displacement $U_y \times 10^2$ (right column). Top row: $\nu = 0.25$. Middle row: $\nu = -0.25$. Bottom row: $\nu = -0.5$.

Kolosov constant, κ_1 and κ_2 , the displacements $u_x \approx u_{x1}$ (for every x) are equal if

$$2\pi h \sinh\left(\pi \frac{y}{a}\right) - a \cosh\left(\pi \frac{y}{a}\right) + a \cosh\left(\pi \frac{y+2h}{a}\right) = 0. \quad (4-4)$$

In the special case when $h = a$, the solution of the transcendental equation is

$$y = \frac{a}{2\pi} \ln\left(\frac{2\pi + 1 - e^{-2\pi}}{2\pi - 1 + e^{2\pi}}\right) \approx -0.686a, \quad (4-5)$$

which can be treated as a sufficiently accurate approximation of the intersection point. Needless to say, the vertical location is independent of both x and ν .

When it comes to the point of zero longitudinal displacement ($U_x = 0$), it moves down as ν is decreased. Because the point corresponds to the nearly horizontal zero isoline mentioned before (see Figure 6, left column), its y -position is similar over the whole range $0 \leq x \leq a$ (see Figure 7). Using again the first term of the series solution, the average horizontal displacement can be defined as

$$u_x^{(\text{avg})} = \frac{1}{a} \int_0^a u_{x1} dx. \quad (4-6)$$

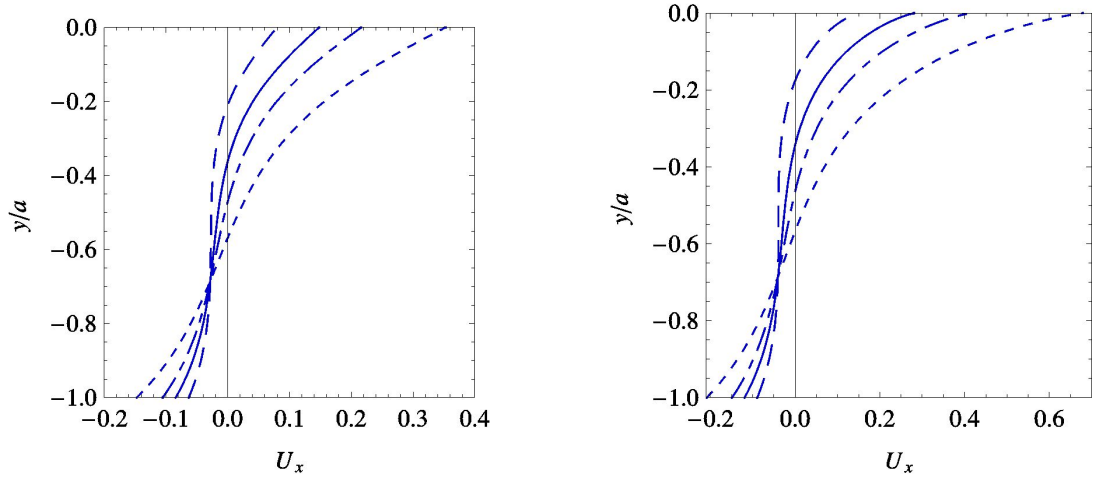


Figure 7. Deplanation of the layer cross-section for $\nu = 0.25$ (dashed), $\nu = 0$ (solid), $\nu = -0.25$ (dot-dashed), and $\nu = -0.75$ (dotted). Left: $x = a/4$ and $x = 3a/4$. Right: $x = a/2$.

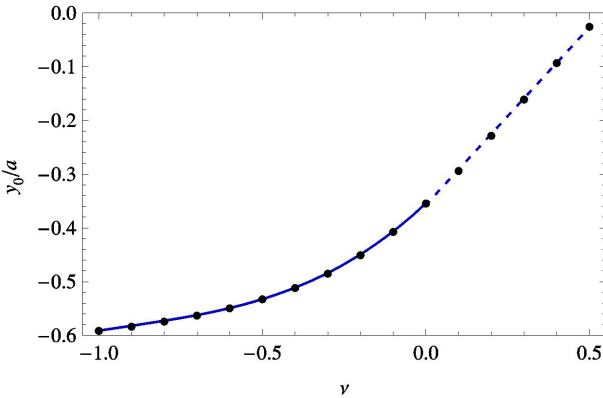


Figure 8. Vertical position of the zero average horizontal displacement versus Poisson’s ratio: approximate solutions (marks); the cubic curve (solid) and line (dotted) fitted in the least-squares sense.

Now, the algebraic equation $u_x^{(\text{avg})}(y) = 0$ can be solved numerically to find the approximate (averaged) vertical position y_0 of the zero point (zero isoline) for $0 \leq x \leq a$ (and $a \leq x \leq 2a$). The solutions for varying Poisson’s ratio within the range $-1 \leq \nu \leq 0.5$ (with the step $\Delta \nu = 0.1$) are shown in [Figure 8](#). This discrete dependence $y_0(\nu)$ can be approximated, for example, by the standard polynomial curve fitting in a least-square sense. Here, two subintervals have been considered separately, related to nonauxetic and auxetic materials ($0 \leq \nu \leq 0.5$ and $-1 \leq \nu \leq 0$). A linear function and a cubic curve have been fitted to the data, respectively. In both cases, the root-mean-square error of the approximations is less than 1% (about 0.22% and 0.47%). It can be concluded that the characteristics become “softer” in the auxetic range, i.e., the value y_0 drops increasingly slower as Poisson’s ratio tends to -1 .

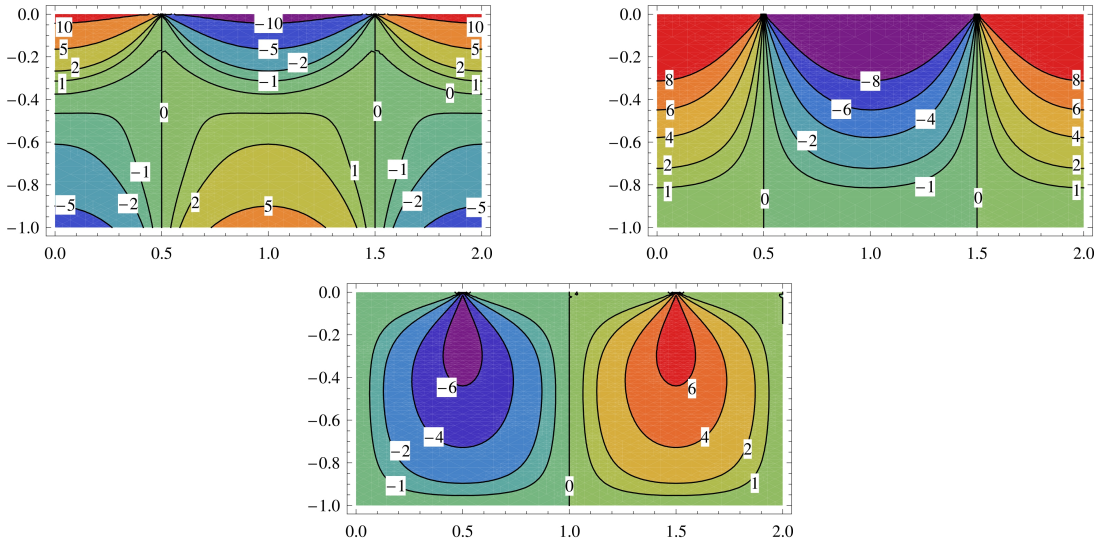


Figure 9. Stress distribution in a rectangular cell. Left: normal stress $S_x \times 10$. Right: normal stress $S_y \times 10$. Bottom: shear stress $S_{xy} \times 10$.

Distributions of normal stress S_x , S_y and shear stress S_{xy} (all scaled by a factor of 10) are presented in [Figure 9](#). Note that the quantities are independent of ν , according to the remark on [\(3-26\)](#) and [\(3-27\)](#). As can be seen, the vertical contours of zero normal stresses correspond to zero contours of U_y . In the case of shear stress, in turn, the zero isoline coincides with the one for $U_x = 0$.

The lack of dependence of the stress field on Poisson's ratio may seem curious. The problem has been considered within the classical linear elasticity framework, for the whole (thermodynamically admissible) range of ν . Thus, one can state that S_x , S_y , S_{xy} are always the same, identical for both the auxetic and conventional materials (homogeneous and isotropic in each case). However, such a solution is not so unusual: results of this nature can arise within linear elasticity [[Timoshenko and Goodier 1951](#); [Timoshenko 1930](#); [Ventsel and Krauthammer 2001](#); [Boresi et al. 1993](#)]. For instance, the analyzed elastic layer problem may be confronted with the case of cylindrical bending of a rectangular plate (finite or infinite). Thus, consider a clamped-clamped thin plate of length a in the x -direction and infinitely long in the z -direction (xz is the middle plane), subjected to a uniform transverse load $p = \text{constant}$ (upward or downward). It is well known that an expression for the plate deflection $u_y(x)$ would include Poisson's ratio (via the flexural rigidity), while the normal stress σ_x would be free of this elastic constant. Obviously, the classical thin plate theory further assumes that $\sigma_y = \sigma_{yz} = 0$ (plane stress relative to the xz -plane), which is too strong a constraint not consistent with our formulation. But even if the stress components σ_y , σ_{yz} are approximately determined through the use of the differential equations of equilibrium (against Kirchhoff's assumptions), they also are not influenced by ν [[Ventsel and Krauthammer 2001](#); [Boresi et al. 1993](#); [Jaeger 1964](#); [Szilard 2004](#)].

4.2. FEM results. Exact solutions, achievable for simple geometry and load cases, are often used to assess accuracy and efficiency of new or modified numerical techniques. Vice versa, a well-established computer method can be applied in order to validate newly developed analytical solutions. Unarguably,

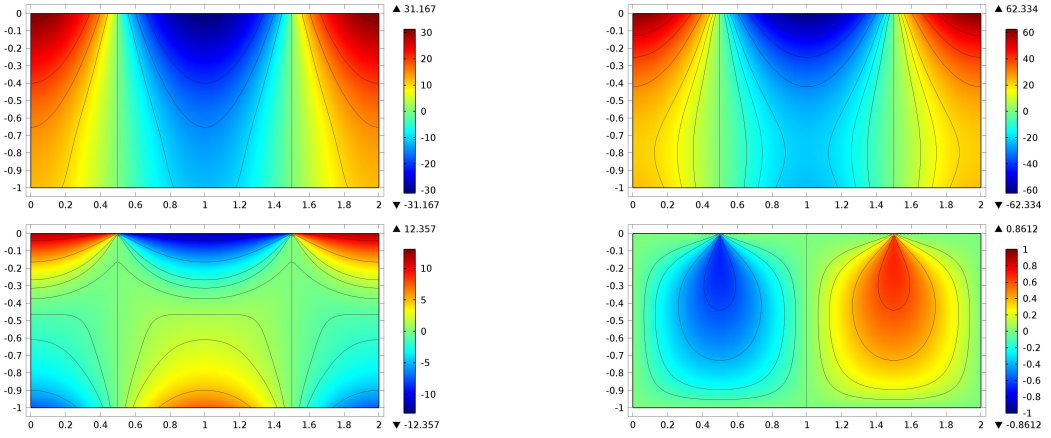


Figure 10. FEM results for a rectangular cell. Top left: $U_y \times 10^2$ for $\nu = 0.25$. Top right: $U_y \times 10^2$ for $\nu = -0.5$. Bottom left: $S_x \times 10$. Bottom right: $S_{xy} \times 10$.

the finite element method (FEM) is one of the most common approaches to modeling and simulation in science and engineering, including solid mechanics. For example, FEM-based reference results were used in [Walczak et al. 2014; Fritzowski and Kamiński 2016] to examine exact solutions or numerical solutions obtained via meshless methods. Similarly, comparative simulations have been conducted for the present case, by means of COMSOL Multiphysics software.

Due to the spatial periodicity of the layer, the linear static analysis is focused on a finite-sized domain, i.e., the rectangular cell:

$$\widehat{\Omega} = \begin{cases} 0 \leq x \leq 2a, \\ -h \leq y \leq 0. \end{cases} \quad (4-7)$$

Apart from boundary conditions (2-7a) and (2-7c), the following ones are imposed on the left and right edges (roller supports):

$$u_x(0, y) = 0, \quad u_x(2a, y) = 0. \quad (4-8)$$

Moreover, two pointwise displacement conditions are introduced as

$$u_y\left(\frac{1}{2}a, 0\right) = 0, \quad u_y\left(\frac{3}{2}a, 0\right) = 0. \quad (4-9)$$

On the one hand, these assumptions can be concluded from the semianalytical results. On the other hand, such a behavior of the loaded surface is a natural consequence of the fact that the resultant of the distributed load on the periodic cell is zero.

A uniform rectangular mesh is generated in the entire domain (a swept mesh). The quadratic quadrilateral finite elements are used. The presented results have been obtained for $n_e = 5000$ finite elements (100×50) and $n_{\text{dof}} = 40602$ degrees of freedom.

The distribution of displacement U_y and stress S_x obtained numerically for $\nu = 0.25$ and $\nu = -0.5$ are shown in Figure 10. Thus, the graphs can be compared to the ones in Figure 6, top row and bottom row, and Figure 9, left and bottom. For convenience, the same isolines have been included in the FEM-based plots. As can be seen, the displacement and stress fields provided by two different methods are in very

ν		0.49	0.25	0	-0.25	-0.5	-0.75	-0.99
U_y^{\max}	semianalytical	0.2119	0.3117	0.4155	0.5194	0.6233	0.7272	0.8269
	FEM	0.2119	0.3117	0.4156	0.5195	0.6233	0.7272	0.8270
U_x^{\max}	semianalytical	0.0215	0.1488	0.2814	0.4140	0.5466	0.6792	0.8064
	FEM	0.0210	0.1484	0.2809	0.4133	0.5457	0.6779	0.8048

Table 1. Semianalytical vs. FEM results: maximal displacements.

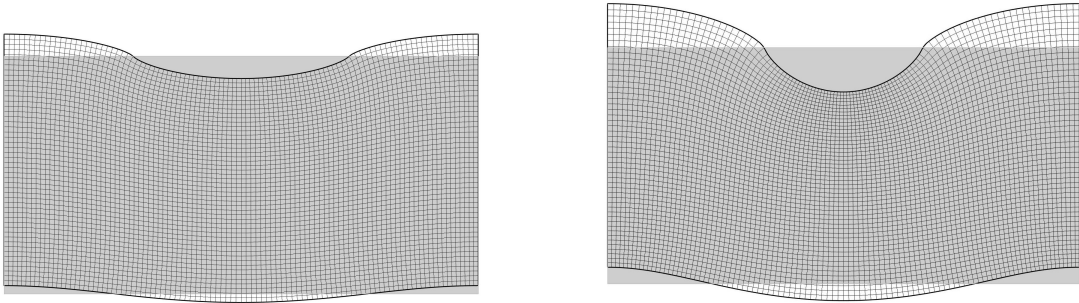


Figure 11. FEM results — deformation of a rectangular cell. Left: $\nu = 0.25$. Right: $\nu = -0.5$.

close agreement with each other. Table 1 contains the maximal displacements U_y^{\max} and U_x^{\max} obtained with FEM ($n_{\text{dof}} = 40602$) and the semianalytical procedure ($n = 50$). It turns out that the values are almost identical.

Deformation of the rectangular cell for $\nu = 0.25$ and $\nu = -0.5$ (drawn at the same scale) can be observed in Figure 11. In full accordance with the analytical results depicted in Figure 4, vertical displacements within the cell increase with decreasing Poisson's ratio.

5. Conclusions

In this paper, elastic deformation of an infinite layer under a periodic load has been considered. The semibounded character of the domain allows for an analytical treatment of the problem. The displacements of the loaded surface and other surfaces of the layer have been presented and discussed. Moreover, the distributions of the displacements as well as the normal and shear stresses in the periodic cell of the domain have been presented. The effect of Poisson's ratio on the system behavior has been analyzed.

Although the Fourier integral transform has been applied, evaluation of the inverse transforms for the displacements and stresses does not require numerical computation of residues, as for example in the case of elastic quarter-space [Fritzowski and Kamiński 2016]. The analytical solution is represented by an infinite single series of relatively simple form. The results indicate quite fast convergence of these series. Furthermore, they are in high agreement with the purely numerical solutions obtained by means of the finite element method (FEM).

It has been demonstrated that the horizontal and vertical displacements of the layer surface grow (in absolute value) with decreasing ν at constant G . In the studied case, the relationship between the system response and Poisson's ratio turns out to be linear. Hence, in the context of contact mechanics, e.g., when

a rigid punch is pressed against an elastic material, one can expect that the indentation depth will be higher for auxetics than for conventional solids. Such behavior seems to contradict the effect of practical importance, highlighted by many authors: the indentation resistance increases with the auxeticity of the material [Sanami et al. 2014; Greaves et al. 2011; Carneiro et al. 2013]. However, in the mathematical description of deformable solids, Young's modulus and Poisson's ratio (E , ν) are usually employed instead of shear modulus and Poisson's ratio (G , ν). When the latter pair is used (as in this paper), the conclusions of a physical nature can change: the application of more auxetic materials (at constant shear modulus) does not necessarily suppress the deformation [Lim 2015]. So, the selection of elastic constants is crucial, and must not be ignored or underestimated by engineers and researchers.

The horizontal displacements of the layer through its thickness have been analyzed carefully. It has been shown that all the deplanation profiles for various values of ν have a common point. Location of the zero point (zero average longitudinal displacement), in turn, is strongly affected by Poisson's ratio. As ν is lowered, the vertical position decreases linearly in the conventional range, and in a cubic manner in the auxetic range. The stress components for the system, in turn, are independent of Poisson's ratio.

The presented semianalytical approach and the results can be a benchmark for future research on, for example, periodic cell structures made of conventional and auxetic materials.

References

- [Alderson and Alderson 2007] A. Alderson and K. L. Alderson, “Auxetic materials”, *Proc. Inst. Mech. Eng. G, J. Aerosp. Eng.* **221**:4 (2007), 565–575.
- [Boresi et al. 1993] A. Boresi, R. Schmidt, and O. Sidebottom, *Advanced mechanics of materials*, 5th ed., Wiley, New York, 1993.
- [Bronsztajn et al. 2004] I. N. Bronsztajn, K. A. Siemiendajew, G. Musiol, and H. Mühlig, *Nowoczesne kompendium matematyki*, PWN, Warszawa, 2004.
- [Carneiro et al. 2013] V. H. Carneiro, J. Meireles, and H. Puga, “Auxetic materials: a review”, *Mater. Sci. (Poland)* **31**:4 (2013), 561–571.
- [Evans and Alderson 2000] K. Evans and K. Alderson, “Auxetic materials: the positive side of being negative”, *Eng. Sci. Educ. J.* **9**:4 (2000), 148–154.
- [Fritzowski and Kamiński 2016] P. Fritzowski and H. Kamiński, “Stress and displacement analysis of an auxetic quarter-plane under a concentrated force”, *J. Mech. Mater. Struct.* **11**:1 (2016), 3–22.
- [Greaves et al. 2011] G. N. Greaves, A. L. Greer, R. S. Lakes, and T. Rouxel, “Poisson's ratio and modern materials”, *Nat. Mater.* **10** (2011), 823–837.
- [Jaeger 1964] L. Jaeger, *Elementary theory of elastic plates*, Pergamon, Oxford, 1964.
- [Jopek and Strek 2015] H. Jopek and T. Strek, “Thermal and structural dependence of auxetic properties of composite materials”, *Phys. Status Solidi B* **252**:7 (2015), 1551–1558.
- [Lim 2015] T. Lim, *Auxetic materials and structures*, Springer, 2015.
- [Nowacki 1970] W. Nowacki, *Teoria niesymetrycznej sprężystości*, PWN, Warsaw, 1970.
- [Prawoto 2012] Y. Prawoto, “Seeing auxetic materials from the mechanics point of view: a structural review on the negative Poisson's ratio”, *Comput. Mater. Sci.* **58** (2012), 140–153.
- [Saada 1974] A. S. Saada, *Elasticity: theory and applications*, Pergamon Unified Engineering Series **16**, Pergamon, New York, 1974.
- [Sadd 2004] M. H. Sadd, *Elasticity: theory, applications, and numerics*, Elsevier, Amsterdam, 2004.
- [Salit and Weller 2009] V. Salit and T. Weller, “On the feasibility of introducing auxetic behavior into thin-walled structures”, *Acta Mater.* **57**:1 (2009), 125–135.

- [Sanami et al. 2014] M. Sanami, N. Ravirala, K. Alderson, and A. Alderson, “Auxetic materials for sports applications”, *Procedia Eng.* **72** (2014), 453–458.
- [Sneddon 1951] I. N. Sneddon, *Fourier transforms*, McGraw-Hill, New York, 1951.
- [Strek et al. 2010] T. Strek, B. Maruszewski, A. Pozniak, and K. Wojciechowski, “Computational modelling of auxetics”, pp. 265–284 in *Finite element analysis*, edited by D. Moratal, Intech, Rijeka, Croatia, 2010.
- [Szilard 2004] R. Szilard, *Theories and applications of plate analysis: classical, numerical and engineering methods*, Wiley, Hoboken, NJ, 2004.
- [Teodorescu 2013] P. P. Teodorescu, *Treatise on classical elasticity: theory and related problems*, Springer, 2013.
- [Timoshenko 1930] S. P. Timoshenko, *Strength of materials, II: Advanced theory and problems*, Van Nostrand, New York, 1930.
- [Timoshenko and Goodier 1951] S. Timoshenko and J. N. Goodier, *Theory of elasticity*, 2nd ed., McGraw-Hill, New York, 1951.
- [Ventsel and Krauthammer 2001] E. Ventsel and T. Krauthammer, *Thin plates and shells: theory, analysis, and applications*, CRC Press, Boca Raton, FL, 2001.
- [Walczak et al. 2014] T. Walczak, G. Sypniewska-Kamińska, B. T. Maruszewski, and K. W. Wojciechowski, “Mesh versus meshless method of elastic displacement determination in a common and an auxetic material”, *Phys. Status Solidi B* **251**:11 (2014), 2225–2232.
- [Zemanian 1965] A. H. Zemanian, *Distribution theory and transform analysis: an introduction to generalized functions, with applications*, McGraw-Hill, New York, 1965.

Received 16 Jan 2018. Revised 26 Jul 2018. Accepted 19 Aug 2018.

HENRYK KAMIŃSKI: henryk.kaminski@put.poznan.pl

Institute of Applied Mechanics, Poznan University of Technology, Poznan, Poland

PAWEŁ FRITZKOWSKI: pawel.fritzkowski@put.poznan.pl

Institute of Applied Mechanics, Poznan University of Technology, Poznan, Poland

JOURNAL OF MECHANICS OF MATERIALS AND STRUCTURES

msp.org/jomms

Founded by Charles R. Steele and Marie-Louise Steele

EDITORIAL BOARD

ADAIR R. AGUIAR	University of São Paulo at São Carlos, Brazil
KATIA BERTOLDI	Harvard University, USA
DAVIDE BIGONI	University of Trento, Italy
MAENGHYO CHO	Seoul National University, Korea
HUILING DUAN	Beijing University
YIBIN FU	Keele University, UK
IWONA JASIUK	University of Illinois at Urbana-Champaign, USA
DENNIS KOCHMANN	ETH Zurich
MITSUTOSHI KURODA	Yamagata University, Japan
CHEE W. LIM	City University of Hong Kong
ZISHUN LIU	Xi'an Jiaotong University, China
THOMAS J. PENCE	Michigan State University, USA
GIANNI ROYER-CARFAGNI	Università degli studi di Parma, Italy
DAVID STEIGMANN	University of California at Berkeley, USA
PAUL STEINMANN	Friedrich-Alexander-Universität Erlangen-Nürnberg, Germany
KENJIRO TERADA	Tohoku University, Japan

ADVISORY BOARD

J. P. CARTER	University of Sydney, Australia
D. H. HODGES	Georgia Institute of Technology, USA
J. HUTCHINSON	Harvard University, USA
D. PAMPLONA	Universidade Católica do Rio de Janeiro, Brazil
M. B. RUBIN	Technion, Haifa, Israel

PRODUCTION production@msp.org


SILVIO LEVY Scientific Editor

See msp.org/jomms for submission guidelines.

JoMMS (ISSN 1559-3959) at Mathematical Sciences Publishers, 798 Evans Hall #6840, c/o University of California, Berkeley, CA 94720-3840, is published in 10 issues a year. The subscription price for 2018 is US \$615/year for the electronic version, and \$775/year (+\$60, if shipping outside the US) for print and electronic. Subscriptions, requests for back issues, and changes of address should be sent to MSP.

JoMMS peer-review and production is managed by EditFLOW® from Mathematical Sciences Publishers.

PUBLISHED BY

 **mathematical sciences publishers**
nonprofit scientific publishing

<http://msp.org/>

© 2018 Mathematical Sciences Publishers

Prediction of springback and residual stress of a beam/plate subjected to three-point bending	QUANG KHOA DANG, PEI-LUN CHANG, SHIH-KANG KUO and DUNG-AN WANG	421
Characterization of CNT properties using space-frame structure	MUHAMMAD ARIF and JACOB MUTHU	443
Analytical approach to the problem of an auxetic layer under a spatially periodic load	HENRYK KAMIŃSKI and PAWEŁ FRITZKOWSKI	463
Stability and nonplanar postbuckling behavior of current-carrying microwires in a longitudinal magnetic field	YUANZHUO HONG, LIN WANG and HU-LIANG DAI	481
Three-dimensional Trefftz computational grains for the micromechanical modeling of heterogeneous media with coated spherical inclusions	GUANNAN WANG, LEITING DONG, JUNBO WANG and SATYA N. ATLURI	505
Uniform stress resultants inside two nonelliptical inhomogeneities in isotropic laminated plates	XU WANG, LIANG CHEN and PETER SCHIAVONE	531
An analytical solution for heat flux distribution of cylindrically orthotropic fiber reinforced composites with surface effect	JUNHUA XIAO, YAOLING XU and FUCHENG ZHANG	543
Strain gradient fracture of a mode III crack in an elastic layer on a substrate	JINE LI and BAOLIN WANG	555
Growth-induced instabilities of an elastic film on a viscoelastic substrate: analytical solution and computational approach via eigenvalue analysis	IMAN VALIZADEH, PAUL STEINMANN and ALI JAVILI	571
Application of the hybrid complex variable method to the analysis of a crack at a piezoelectric-metal interface	VOLODYMYR GOVORUKHA and MARC KAMLAH	587